Influence of N-Doping on the Structure and Electronic Properties of Titania Nanoparticle Photocatalysts

ARTICLE *in* THE JOURNAL OF PHYSICAL CHEMISTRY B · SEPTEMBER 2006

Impact Factor: 3.3 · DOI: 10.1021/jp0624451 · Source: PubMed

Influence of N-Doping on the Structure and Electronic Properties of Titania Nanoparticle Photocatalysts

Silvana J. Stewart,[†] Marcos Fernández-García,[‡] Carolina Belver,[‡] B. Simon Mun,[§] and Félix G. Requejo*[,†,||]

Departamento de Física, Fac. Ciencias Exactas, Universidad Nacional de La Plata and IFLP (CONICET), C. C. 67 - 1900 La Plata, Argentina, Instituto de Catálisis y Petroleoquímica, CISC. 49706 Cantoblanco, Madrid, Spain, Advanced Light Source, LBNL, Berkeley, California 94720, and INIFTA (Fac. Ciencias Exactas, UNLP and CONICET), C. C. 16 suc. 4 - 1900 La Plata, Argentina

Received: April 20, 2006; In Final Form: June 23, 2006

N-containing TiO_2-based nanostructured materials (average particle size ~10 nm) with an anatase-type structure were investigated using oxygen (O) K-edge and titanium (Ti) K- and L-edge X-ray absorption near-edge spectroscopy (XANES). The Ti K pre-edge features indicate that samples predominantly contain $^{[6]}$Ti with some $^{[5]}$Ti, and there is no evidence for $^{[4]}$Ti. We observed that those samples with a larger fraction of Ti in a fivefold coordination, that is, with a significant number of oxygen vacancies, also present a modified Ti environment at the medium-range scale. The presence of these defects drastically modifies the electronic structure of the conduction band, as evidenced by the O K XANES spectra, but does not result in the presence of reduced Ti^{3+} states. We discuss the influence of N-doping on titania nanoparticles and their structure, electronics and photocatalytic activity.

Introduction

Anatase-type TiO_2 (a-TiO_2) has attracted much attention because of its significant technological interest due to its potential application as photocatalysts for the elimination of organic compounds in polluted environment. Research efforts have been focusing on enhancing the photocatalytic efficiency and searching for TiO_2-based materials that can be active under visible light excitation[1−3]. Recently, it has been proposed that anionic doping of TiO_2 with N would narrow the anatase band gap, thus allowing the absorption of visible light.[4−6] However, the mechanisms that originate the absorption edge to be shifted to a longer-wavelength region are still under discussion. The mixing of the N 2p and O 2p states has been alternatively proposed, where the N 2p levels form an isolated narrow band within the band gap just above the valence band without narrowing the band gap.[6−8]

Previously, we have reported the synthesis and characterization of N-containing TiO_2 nanostructures and studied their photocatalytic behavior under sunlight excitation.[1,2] We found that N occupies substitutional and interstitial sites replacing oxygen in the anatase structure and also generates, even for very low N-content, a vast amount of oxygen vacancies. The photocatalytic activity correlates with an optimum number of vacancies, but additional insight into the electronics of the Ti and O atoms in N-doped titania is necessary for a realistic connection between electronics and the catalytic process.

To this aim, we propose the study of the electronics in anatase doped with N. X-ray absorption near-edge structure (XANES) studies at O K-edges, Ti L-edges, and Ti K-edges were performed to ascertain this subject. We discuss the influence of defects generated by N-doping on the local- and medium-range order around Ti in N-containing TiO_2 nanostructures and how this can influence their photocatalytic activity.

Experimental Section

N-containing TiO_2-based materials were prepared by modifying a titanium iso-propoxide precursor with an N-containing molecule (methoxyethylamine) forming different Ti precursors to obtain TiO_2-based photocatalysts by using a reverse micelle microemulsion method. The resulting microemulsion was stirred for 24 h, centrifuged, rinsed with methanol, and calcined using three different treatments always consisting on a ramp at 1 °C min^{-1} with 2 h plateaus at 200 and 450 °C, the latter being the final temperature of treatment. Treatments differ in the specific point/temperature where O_2 (20 vol %) is added to the Ar, being incorporated from the beginning (treatment called "1") and at the onset of the first ("2") and second plateau ("3"). Samples were called with a prefix, which provides information concerning the Ti/methoxyethylamine molecular ratio, followed by the letter M and a subfix between 1 and 3, which declares the thermal treatment suffered by the sample (e.g., M3, 2M1, 2M2, 2M3, 1/2M3). The 2M sample was also studied without calcination treatment (2Msc). Reference samples were produced by using the Ti isopropoxide as precursor (T1) or obtained from BDH (bulk TiO_2; particle size 80 nm). Full details of sample preparation procedure and most important structural/morphological characteristics can be found elsewhere.[2] Here we only mention that all samples display anatase structure by X-ray diffraction and contain N below 0.2 atom %.[2]

Ti K-XANES experiments were performed in transmission mode by using a Si(111) monochromator at the XAS1 beamline of the LNLS (Laboratorio Nacional do Luz Sincrotron, Campinas, Brazil). The harmonic contamination of the beam

* Corresponding author. Address: Departamento de Física, Fac. Ciencias Exactas, Universidad Nacional de La Plata and IFLP (CONICET), C. C. 67 - 1900 La Plata, Argentina. E-mail: requejo@fisica.unlp.edu.ar.

[†] Departamento de Física, Fac. Ciencias Exactas, Universidad Nacional de La Plata and IFLP (CONICET).

[‡] Instituto de Catálisis y Petroleoquímica.

[§] Advanced Light Source, LBNL.

[||] INIFTA (Fac. Ciencias Exactas, UNLP and CONICET).

10.1021/jp0624451 CCC: $33.50
Published on Web 07/29/2006

was lower than 1%, the beam energy was 1.37 MeV, and the energy resolution was 0.8 eV. The beam intensities were measured using ionization chambers filled with He at room temperature and atmospheric pressure. The energy-scale calibration was performed measuring in transmission mode a Ti-foil between the second and third ionization chambers. The edge position was determined by fixing the first zero of the second derivative at 4966 eV. The XANES spectra analysis was performed by pre-edge background subtraction followed by a normalization procedure considering the extended region (above 5050 eV).

XANES spectra at low energy (L-Ti and O-K edges) were measured at the Advanced Material Chamber, located at the bending magnet beamline 9.3.2 of Advanced Light Source (ALS) in Lawrence Berkeley National Laboratory (LBNL). The entire XANES measurements were carried out in total electron yield (TEY) mode at room temperature under UHV condition, which had the base pressure of low 10^{-10} Torr. The energy resolution of beamline was set to ~0.15 eV, and the angle of incident beam to the sample surface for all XANES spectra was adjusted to 45°. The calibration of photon energy was performed by using standard anatase TiO_2 for both Ti and O edges. Powder samples were pressed onto Indium foils and mounted on a molybdenum sample holder. All measured spectra were normalized to photon flux, obtained from the current yield of a clean Au grid, placed before samples. After background discount, the spectra were normalized to the spectral area between 445 and 468 eV and 522 and 552 eV for L-Ti and O-K edges, respectively. To obtain the peak parameters, we fitted the experimental spectra to Lorentzian functions.

Results and Discussion

Pre-Edge Features of Ti K-Edge XANES. The Ti K-edge spectra of the samples resembled those found in anatase-like compounds, irrespective of the treatment.[1] In anatase, Ti atoms are six-coordinated to oxygen having a D_{2d} punctual symmetry. Thus, the pre-edge Ti-K XANES structure arises formally from a 1s to 3d dipole symmetry forbidden transition. The final excited states are described by a mixing of 4p and 3d orbitals from Ti central atom and Ti higher shells.[9−13] This orbital mixing only takes place in noncentrosymmetric environments. Because the degree of mixing depends on Ti−Ti distances, the pre-edge peak intensities are affected by the particular medium-range structure of the sample. Although the origin of the individual contributions to this pre-edge structure for titanium oxides is still under discussion,[9,12−16] empirical analyses have been extensively useful for gaining information related to the coordination geometry of Ti, cationic valence, and medium-range-type ordering of the Ti-containing oxides.[11,17,18] These analyses are based on the existing correlation between the normalized height and energy peak positions with the coordination number of Ti.[11] Indeed, it has been established that the intensity of the pre-peaks increases as the central Ti atom site becomes more noncentrosymmetric due to the consequent increase of the degree of orbital p−d mixing. Although most of the experimental and theoretical works have identified three pre-peaks (labeled A1, A3, and B, see Figure 1) of the Ti K-pre-edge region for anatase,[10,12,14,16] high-energy resolution allows us to distinguish a forth peak, A2, which appears as a shoulder at the low-energy side of A3.[9,17,19] After the background subtraction and normalization procedures, we fitted the pre-edge region to four Lorentzian lines A1, A2, A3, and B plus an extra peak that accounts for the edge rising (see Figure 1). To obtain the middle peak parameters, we have considered

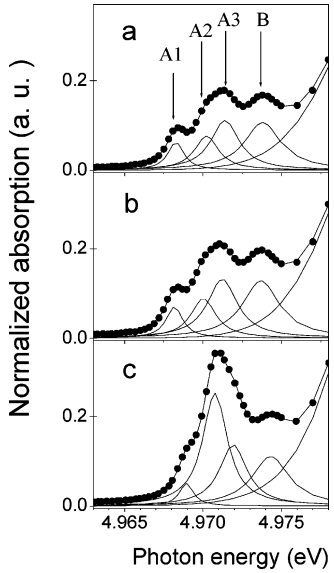

Figure 1. Experimental data at pre-edge region of Ti-K absorption XANES spectra (circles) and fitting (line) with four Lorentzian functions. (a) Bulk anatase-TiO_2, (b) 2M2, and (c) 2Msc. Spectra b and c are representative of the high and low coordination state for Ti in N-doped nanostructured TiO_2 samples, respectively.

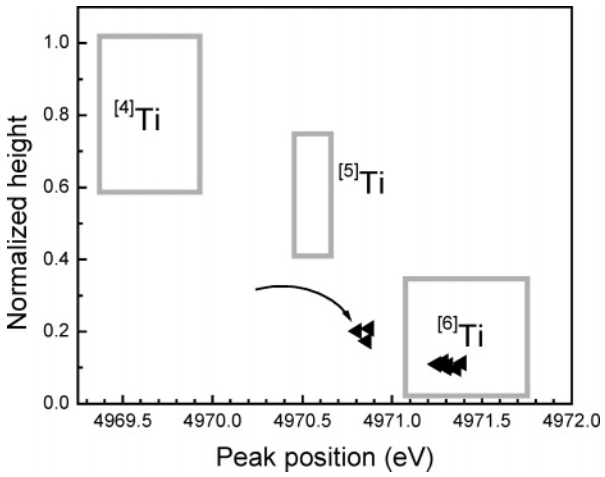

Figure 2. Plot of the normalized height of pre-peaks vs absolute energy positions of higher pre-peaks that result after the fitting procedure at Ti K-edge XANES spectra. Rectangles indicate the expected region for each Ti coordination.[11] The arrow indicates the position and intensities corresponding to O vacancies, enriched samples, and triangles inside the rectangle correspond to samples without O vacancies.

the average heights and peak positions taking into account both A2 and A3 peaks weighted by their area's intensities as $A_{Ai}/(A_{A2} + A_{A3})$, $i = 2, 3$, where A_{Ai} denotes the peak area of peak Ai. These results are presented together with additional data taken from the literature[11] (Figure 2). Although for most of the samples these peak parameters are included inside the sixfold region, those for samples 2Msc, 1/2M3, and M3 lie outside the [6]Ti region and comprehend a zone to be expected for a sample containing a [6]Ti and [5]Ti combination.[10] In addition, the intensity ratio A_{A2}/A_{A3} increases for those samples (Figure 1). These results reveal that they contain a mixture of penta- and hexa-coordinated Ti atoms, while no evidence for tetrahedrally coordinated Ti is obtained.

Previously reported EXAFS analysis also suggested the presence of pentacoordinated titanium in a higher percentage for samples 2Msc, 1/2M3, and M3.[1] Moreover, although the anatase-like structure is preserved for all of the samples (see

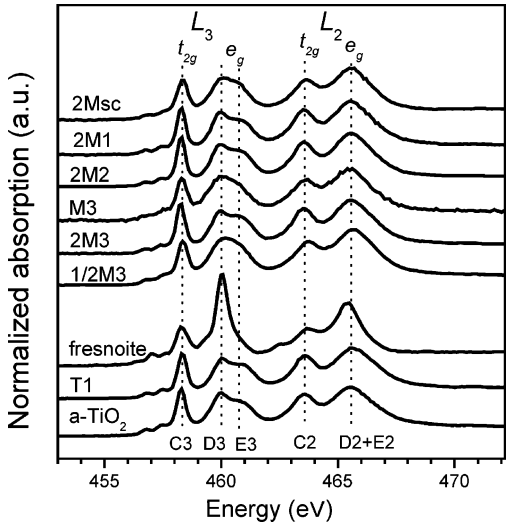

Figure 3. Ti L-edge XANES spectra of N-TiO_2 samples and reference compounds. Energy of the known electronic transitions are indicated by dotted vertical lines and specified by the labels.

XRD and Raman results in ref 2), strong deviations were observed for the first Ti−Ti coordination shell. In these cases, the reduction on the second shell coordination number, the shrinking of Ti−O bond distances, and the absence of third shell contribution observed for sample M3 not only indicate the presence of point-defects (i.e., oxygen vacancies) but also an additional modification of the medium-range ordering.

Previous works reported that as the anatase particle size decreases the middle peak contribution at the pre-edge region increases[10,19,20] (see peaks A2 and A3 in Figure 1). This was interpreted as due to the large fraction of Ti atoms at the surface, which present a pentacoordinated geometry accounting for distorted environments.[20] Our anatase nanostructures display an average particle size of 10.0 ± 2.5 nm; thus, the dissimilar fraction of fivefold coordinated Ti atoms cannot be assigned to a dominant nanometric size effect. However, Wu et al.[21] have also detected the same variation of the pre-edge features for anatase particles of 4.5 nm, but they were attributed to the particular medium-range structure of the nanoparticles. It seems that, in our case, the presence of $^{[5]}$Ti is associated with oxygen vacancies whose relative fraction depends on the calcination treatment conditions and is not correlated with the N impurity level present in the solid catalyst. A similar effect has been reported recently on TiO_2 rutile(110) and anatase(101) single crystals after doping with N.[7]

Ti $L_{2,3}$-Edge XANES. Ti L-XANES spectra, characterized by low intrinsic broadening and better energy resolution in comparison to K-edge, provide detailed information about the local Ti bonding configuration and medium-range effects. Therefore, the inspection of the L-Ti edge gives complementary data to those obtained from the K−Ti pre-edge features about the Ti environment and the particular electronic properties of Ti compounds.[22−24] The Ti 2p XANES spectra (Figure 3) consist of two sets of peaks, L_3 and L_2, separated by 5 eV. They correspond to electronic transitions from the $2p_{3/2}$ and $2p_{1/2}$ sates to a 3d excited state of Ti atoms, respectively.[9,23,24] The peaks of L_2 are broader due to the shorter lifetime of its excited state, because it can decay to the 2p3/2 state through an Auger process.[23] As the crystal field splits the 3d state of Ti into two levels, t_{2g} and e_g, each L peak presents two contributions C3 (C2) and D3 (D2), respectively (Figure 3). Furthermore, the e_g peak has an asymmetry or an additional splitting (peaks E3 and E2) that has been attributed to distortions from O_h symmetry by de Groot et al.[23] However, other authors have pointed out that the e_g splitting would originate from the effect of the Ti second coordination shell.[9,24,25] The different relative intensities between D and E peaks indicate different distortions from octahedral symmetry and this, for instance, allows us to distinguish between anatase and rutile TiO_2 phases.[22] Compounds with pentacoordinated Ti (e.g., fresnoite) display a noticeable decrease of the relative intensity C3/D3 (and C2/D2), in addition to the appearance of an extra peak at 462.5 eV (Figure 3).

TABLE 1: Positions of the Peaks in Ti $L_{2,3}$ XANES Spectra of N-Doped TiO_2 Samples and References[a]

sample	C3 (eV)	D3 (eV)	E3 (eV)	Δ_1 (eV)	C3/D3	E3/D3	Δ_2 (eV)	C2 (eV)	D2 (eV)	E2 (eV)
TiO_2	458.3	459.9	460.8	2.2	0.9	2.1	2.2	463.5	465.5	466.4
T1	458.3	460.0	460.9	2.3	1.0	2.3	2.3	463.6	465.5	466.4
2Msc	458.4	460.0	460.7	2.0	0.8	1.3	2.0	463.6	465.5	466.4
2M1	458.3	459.9	460.8	2.2	1.0	2.9	2.2	463.5	465.5	466.4
2M2	458.3	459.9	460.9	2.3	0.8	2.3	2.3	463.5	465.5	466.2
M3	458.3	459.9	460.7	2.0	0.8	1.0	2.0	463.5	465.5	466.2
2M3	458.3	459.9	460.8	2.2	0.9	2.2	2.2	463.5	465.5	466.3
1/2M3	458.3	459.9	460.7	2.1	0.8	1.4	2.1	463.5	465.5	466.7

[a]The labels of the peaks are as indicated in Figure 3. Δ_1 and Δ_2 represent the distance between E3 and D3, E2 and D2 peaks, respectively. C3/D3 and E3/D3 are the intensity ratios.

Spectra recorded at Ti L-edges for N-doped TiO_2 samples are also shown in Figure 3. We observe that the spectra are similar to those of anatase for most of the samples, the lines being broader as compared to the reference sample. In particular, spectra of samples 2Msc, 1/2M3, and M3 show the e_g peak less resolved. There is also a slight decrease of the distance between C3 (C2) and D3 + E3 (D2 + E2) peaks, namely, Δ_3 (Δ_2) belonging to L_3 (L_2) (see Table 1). In addition, the relative intensity E3/D3 considerably increases for this set of samples, whereas no substantial changes were noticed in the C3/D3 ratio. A decrease of the relative intensities E3/D3 has also been observed for amorphous a-TiO_2 and TiO_2 aerogels with anatase local structure[25] when compared to bulk anatase. In these cases, the less resolved e_g band has been related to the deficient or nonexistent long-range ordering.

We also observe that the line-width at half-maximum of peak C3 for 2Msc, 1/2M3, and M3 samples increases about 50% with respect to the anatase reference. For the rest of the samples, the width increment is only about 10%. Because C3 accounts for the transition to the t_{2g} band is less sensible to local distortion of the Ti environment, the broadening can be caused by different sites occupied by Ti atoms.[22] Moreover, the same trend can be observed in fresnoite (Figure 3), which has Ti in a fivefold coordination.

O K-Edge XANES. The oxygen 1s XANES spectra of TiO_2 reflect the density of unoccupied electronic states of 2p type. Because the O 2p orbitals are hybridized with the Ti 3d and 4sp ones, they also account for these metal states.[26−28] Two energy regions can be distinguished (see Figure 4): (i) the region from 530 to 535 eV, which is associated to transitions to the O(2p)-Ti(3d) band. As the crystal field splits the 3d levels into t_{2g} and e_g this gives rise to two contributions labeled A and B, respectively. (ii) the region in the 540 to 550 eV range that includes transitions to the O 2p antibonding state (peak C) and O(2p)-Ti(4sp) band (peak D).[27]

Figure 4 shows the XANES O-K spectra of N-doped TiO_2 samples. For samples 2Msc, 1/2M3, and M3, the spectra show that the t_{2g} and e_g contributions are less resolved and, in addition, the distance between these peaks (Δ_{AB}) that is related to the ligand field splitting increases slightly (Table 2) mainly because

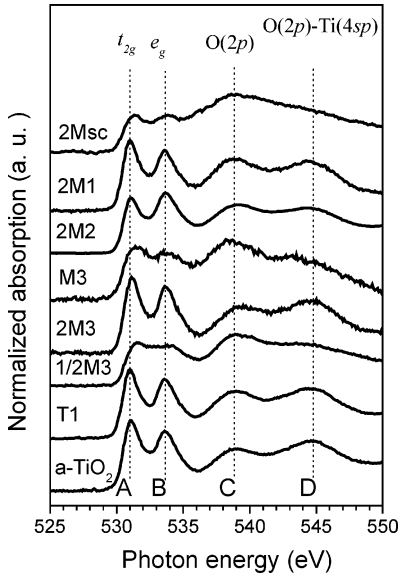

Figure 4. O K-edge XANES spectra of N-doped TiO_2 samples and references. Energy of the known electronic transitions are indicated by dotted vertical lines and specified by the labels.

TABLE 2: Positions of the Peaks in O-K XANES Spectra of N-Doped TiO_2 Samples and References[a]

sample	A (eV)	B (eV)	Δ_{BA} (eV)	C (eV)	D (eV)
TiO_2	531.1	533.8	2.7	538.9	544.6
T1	531.0	533.8	2.8	538.8	544.5
2Msc	531.2	534.1	2.9	538.7	543.4
2M1	531.0	533.8	2.8	538.7	544.6
2M2	531.1	533.9	2.8	539.0	544.5
M3	531.2	534.2	3.0	538.3	544.3
2M3	531.1	533.9	2.8	539.2	544.6
1/2M3	531.4	534.3	2.9	538.8	543.8

[a] The labels of the peaks are as indicted in Figure 4. Δ_{BA} is the distance between A and B peaks.

of the shifting of B peak to higher energies. The spectra corresponding to the rest of the samples are similar to the anatase reference. The high-energy-region feature is sensitive to medium-range interactions.[26,27] Thus, in parallel to the influence on the e_g band (peak B, Figure 4), stronger evidence of the distortion of the Ti environment at medium-range evolves from the high-energy region of O-K XANES spectra of the 2Msc, 1/2M3, and M3 samples, where an important increment of the peak that corresponds to the antibonding O(2p) transition is observed but a moderate decrease is detected at the O(2p)-Ti(4sp) peak (see Figure 4, peaks C and D, respectively). Previously, strong variations of the O K-edge features were reported for anatase nanoparticles (~4 nm) produced by flame synthesis.[29] In such case, apart from the lack of resolution of the t_{2g} and e_g peaks, an important increment of the intensity of the high-energy-region peaks was observed, the C and D peaks being much less distinguishable. These features concerning the high-energy region were attributed to the lack of long-range ordering. The same was concluded for TiO_2 aerogeles having an amorphous anatase,[25] although in this case the relative intensity of the high-energy region is not so pronounced.

It is worth mentioning that such an increment of the O (2p) contribution at the O K-edge XANES spectrum, to our knowledge, was not reported before. Because the XRD data (not shown here), as well as the present XANES characterization, do not indicate the presence of new species (like TiN), this contribution constitutes a direct experimental evidence about the new electronics present at O atoms because of the N-doping in nanostructured anatase.

Nanostructured N-TiO_2: Defect Properties. The X-ray diffraction data of these N-containing TiO_2 nanocrystals of similar sizes and N content showed that all of the samples present a long-range structural ordering compatible with an anatase-type structure. The EXAFS[1] (not showed here) and XANES results (Figure 3) also reflect that these samples are locally more similar to anatase, but the presence of point defects originated by oxygen vacancies alters the short-range Ti environment (Figure 1). Moreover, the presence of point defects produces a significant alteration of the medium-range order with a significant decrease, between 40 and 60% of the first Ti−Ti cation coordination number and further shells. The larger the number of oxygen vacancies, the smaller the cation−cation and further shells' coordination numbers.[1,2]

The strong structural effects of N doping, with particular attention to the defect formation mechanism, have been discussed recently in model rutile and anatase TiO_2 single crystals.[7] Significant differences are, however, encountered between such model systems and our real catalysts. A first important point is that samples produced by ion implantation are not thermally stable and evolve under heating, at least in terms of the creation of oxygen vacancies and concomitant presence of Ti^{3+} after thermal treatment under oxygen at 750 °C.[7] Here we can show that oxygen vacancies existing in the solid precursor 2Msc are reasonably stable throughout heating treatments in oxygen, at least under treatment 3. This is nicely illustrated in Figure 2, which, as said before, would indicate that 1/3 of Ti have an oxygen vacancy in their first coordination shell. Also, because the energy position of the absorption edge is sensitive to the oxidation state, the data shown in Figure 3 give evidence that no significant Ti^{3+} quantity is present in our samples. This means that, in real catalysts, charge compensation is intimately linked with a medium-range structural effect that seems to involve both anion and cation vacancies. This is discussed further below. In our case, the local order alteration is therefore limited to the presence of $^{[5]}$Ti and concomitant oxygen vacancies with electronic implications restricted to a change in (Ti) e_g and t_{2g} transition intensities, as shown by the Ti $L_{2,3}$ and O K-edge XANES spectra. The broadening of the spectra at the O K-edge may show a tailing effect at the onset, which could be associated with the presence of band gap states coming from a residual quantity of Ti^{3+} but certainly not in the amount expected for the weight factor of $^{[5]}$Ti (equal to 1/3). The model and our real catalyst systems do, however, agree in the fact that the number of oxygen vacancies is huge and not correlated to the N content of the solid (below 0.2 atom % in our case).[1,2,7] This latter fact additionally indicates that compensation of charges occurs over long distances,[6,7] as was also proven in samples subjected to treatment "3" by the low coordination Ti−Ti (and higher shells) numbers showed by EXAFS.[1] In the case of the model TiO_2 systems, such long-range effects produce a rather strong surface reconstruction.[7] Electronically, the medium-range organization around titanium in those samples with cationic vacancies mainly influences the Ti e_g peaks, displacing the average position at higher energies as shown by both the Ti $L_{2,3}$ and O K-edge XANES spectra (Figures 3 and 4). A main point is, however, the apparent increase of O(2p) antibonding states and the concomitant diminishing of O(2p)-Ti(3d/4sp) states at the O K-edge (Figure 5), which may be associated with a somewhat lower Ti−O interaction degree, affecting the bond ionicity and losing band "delocatization". The Ti e_g destabilization may also be inter-

preted as a reduction of covalency effects within the crystal structure. The long-range structural effects of N-doping may thus imply a somewhat larger Ti and O electronic density localization degree.

Role of Defects and Electronic Structure on Catalytic Properties of N-TiO_2. Previously, we have identified the presence of substitutional, $(CN)^{n-}$-type, and interstitial, NO^+-type, N-containing impurities on the samples, the percentage of N content being rather small in all cases.[1,2] The presence of both types of impurities would implicate a rather ill-defined system, which would be the main cause of the peak broadening effects (pre-edge and continuum resonances) detected at Ti and O edges. Nevertheless, samples 2M3 and M3 display significant activity with respect to the T1 and other TiO_2 references. A point made in our previous studies is that there is no simple correlation with a specific N impurity (substitutional or interstitial), total N-related impurities and/or point defects (oxygen vacancies), and photocatalytic activity.[1,2] On the basis of UV−visible spectra, we propose that complex vacancy−impurity electronic interactions producing the existence of band gap states 2.0−2.5 eV from the valence edge may be involved in the photoactivity enhancement. Our present studies may, however, allow envisaging additional electronic effects potentially affecting photoactivity.

As an important result, we have not detected a significant number of Ti^{3+}-related gap states that may act as hole-trapping centers and, thus, degrade photocatalytic properties. This reduced Ti species was detected in model systems with the presence of substitutional N species[7] and would suggest that several N-containing systems with different structural and electronic situations may in fact be considered to explain the results already published in the literature. In our systems, apart from the nonlocalized gap states described before, we found that systems with a significant number of vacancies, for example, M3, and with strong lacking of medium-range order would not maximize catalytic activity, despite the practical absence of Ti^{3+}. This can be correlated with the fact that such a situation favors localization of electronic states by increasing both the crystal ionicity and the structural disorder. Indeed, the O K-edge shows this for the conduction band, a fact that will negatively impact over the hole lifetime and catalytic activity.

In conclusion, the tradeoff between positive and negative electronic effects induced by the presence of N-doping-derived defects is clearly positive in the case of the presence of noninteracting oxygen vacancies. In our case, this beneficial effect may be grounded in the existence of impurity−vacancy-derived gap states without the concomitant presence of Ti^{3+} recombination centers. The case of samples with mutually interacting defects, showing middle- and long-range structural effects (accounting for a significant depletion of second but particularly third and further coordination numbers) may, however, produce detrimental effects coming from the increase in crystal ionicity and lower charge carrier delocalization under light excitation.

Conclusions

We have investigated the electronic structure of N-containing a-TiO_2 nanoparticles prepared by microemulsion, through X-ray absorption spectroscopy at O K-edges, Ti L-edges, and Ti K-edges. The samples are locally more similar to anatase, but the presence of points defects originated by oxygen vacancies alters the short-range Ti environment. Those samples with a larger fraction of Ti in a fivefold coordination also present a modified Ti environment at the medium-range scale. From an electronic point of view, the medium-range organization around titanium in those samples with cationic vacancies mainly influences the Ti e_g peaks. In these cases, we also observed an important increment of peak intensities that corresponds to the antibonding O(2p) transition in the O K-edge, probably associated with a lower Ti−O interaction degree. The results also showed that the absence of a significant Ti^{3+} quantity in all samples. This would imply that in real catalysts charge compensation is linked with a medium-range structural effect, which probably involves both anion and cation vacancies.

Acknowledgment. We appreciate financial support by ANPCYT PICT no. 06-17492, Argentina; CYCIT CTQ2004-03409, España; CSIC-CONICET collaborative research agreement no. 2004AR0070 and CONICET PIP no. 6075 and LNLS synchrotron, Campinas, Brazil (under project D04B - XAFS1 - 3492).

References and Notes

(1) Belver, C.; Bellod, R.; Stewart, S. J.; Requejo, F. G.; Fernández-García, M. *Appl. Catal., B* **2006**, *65*, 309.
(2) Belver, C.; Bellod, R.; Fuerte, A.; Fernández-García, M. *Appl. Catal., B* **2006**, *65*, 301.
(3) Fuerte, A.; M. Hernández-Alonso, D.; Martínez-Arias, A.; J. Conesa, C.; Soria, J.; Fernández-García, M. *J. Catal.* **2002**, *212*, 1.
(4) Zhao, J.; Chen, C.; Ma, W. *Top. Catal.* **2005**, *35*, 267.
(5) Anpo, M. *J. Catal.* **2003**, *216*, 233.
(6) Asahi, R.; Morikawa, T.; Ohwaki, T.; Aoki, K.; Taga, Y. *Science* **2001**, *293*, 269.
(7) Batzill, M.; Morales, E. H.; Diebold, U. *Phys. Rev. Lett.* **2006**, *96*, 026103.
(8) Di Valentin, C.; Pacchioni, G.; Selloni, A.; Livraghi, S.; Giamello, E. *J. Phys. Chem. B* **2005**, *109*, 11414.
(9) Brydson, R.; Sauer, H.; Engel, W.; Thomas, J. M.; Zeitler, E.; Kosugi, N.; Kuroda, H. *J. Phys.: Condens. Matter* **1989**, *1*, 797.
(10) Chen, L. X.; Rajh, T.; Wang, Z.; Thurnauer, M. C. *J. Phys. Chem. B* **1997**, *101*, 10688.
(11) Farges, F.; Brown, G. E., Jr.; Rerh, J. J. *Phys. Rev. B* **1997**, *56*, 1809.
(12) Ruiz-López, M. F.; Muñoz-Páez, A. *J. Phys.: Condens. Matter* **1991**, *3*, 8981.
(13) Grunes, L. A. *Phys. Rev. B* **1983**, *27*, 2111.
(14) Uozumi, T.; Okada, K.; Kotani, A.; Durmeyer, O.; Kappler, J. P.; Beaurepaire, E.; Parlebas, J. C. *Europhys. Lett.* **1992**, *18*, 85.
(15) Cabaret, D.; Joly, Y.; Renevier, H.; Natoli, C. R. *J. Synchrotron Radiat.* **1999**, *6*, 258.
(16) Wu, Z. Y.; Ouvrard, G.; Gressier, P.; Natoli, C. R. *Phys. Rev. B* **1997**, *55*, 10382.
(17) Matsuo, S.; Sakaguchi, N.; Wakita, H. *Anal. Sci.* **2005**, *21*, 805.
(18) Romano, C.; Paris, E.; Poe, B. T.; Giulli, G.; Dingwell, D. B.; Mottana, A. *Am. Miner.* **2000**, *85*, 108.
(19) Luca, V.; Djajanti, S.; Howe, R. F. *J. Phys. Chem. B* **1998**, *102*, 10650.
(20) Chen, L. X.; Rajh, T.; Jäger, W.; Nedeljkovic, J.; Thurnauer, M. C. *J. Synchroton Radiat.* **1999**, *6*, 445.
(21) Wu, Z. Y.; Zhang, J.; Ibrahim, K.; Xian, D. C.; Li, G.; Tao, Y.; Hu, T. D.; Bellucci, S.; Marcelli, A.; Zhang, Q. H.; Gao, L.; Chen, Z. Z. *J. Appl. Phys. Lett.* **2002**, *80*, 2973.
(22) de Groot, F. M. F.; Figueiredo, M. O.; Basto, M. J.; Abbate, M.; Petersen, H.; Fuggle, J. C. *Phys. Chem. Miner.* **1992**, *19*, 140.
(23) de Groot, F. M. F.; Fuggle, J. C.; Thole, B. T.; Sawatzky, G. A. *Phys. Rev. B* **1990**, *41*, 928.
(24) Crocombette, J. P.; Jollet, F. *J. Phys. Condens. Matter* **1994**, *6*, 10811.
(25) Kucheyev, S. O.; van Buuren, T.; Baumann, T. F.; Satcher, J. H., Jr.; Willey, T. M.; Meulenberg, R. W.; Felter, T. E.; Poco, J. F.; Gammon, S. A.; Terminello, L. J. *Phys. Rev. B* **2004**, 69, 245102.
(26) de Groot, F. M. F.; Grioni, M.; Fuggle, J. C.; Ghijsen, J.; Sawatzky, G. A.; Petersen, H. *Phys. Rev. B* **1989**, *40*, 5715.
(27) de Groot, F. M. F.; Faber, J.; Michiels, J. J. M.; Czyzyk, M. T.; Abbate, M.; Fuggle, J. C. *Phys. Rev B* **1993**, *48*, 2074.
(28) Soriano, L.; Ahonen, P. P.; Kauppinen, E. I.; Gómez-García, J.; Morant, C.; Palomares, F. J.; Sánchez-Agudo, M.; Bressler, P. R.; Sanz, J. M. *Monatsh. Chem.* **2002**, *133*, 849.
(29) McCormick, J. R.; Zhao, B.; Rykov, S. A.; Wang, H.; Chen, J. G. *J. Phys. Chem. B* **2004**, *108*, 17398.